Powder Technology 417 (2023) 118258

Contents lists available at ScienceDirect

Powder Technology

journal homepage: www.journals.elsevier.com/powder-technology

Dynamic behaviors of bubble formation on submerged micro-capillary under constant flow conditions

Xiang Wang [a], Minhang Song [a], Shuiqing Li [b], Yun Huang [a,*]

[a] State Key Laboratory of Multiphase Complex Systems, Institute of Process Engineering, Chinese Academy of Sciences, Haidian District, Beijing 100190, China)
[b] Key Laboratory for Thermal Science and Power Engineering of Ministry of Education, Department of Thermal Engineering, Tsinghua University, Beijing 100084, China

HIGHLIGHTS

- Bubble departure volume decreased with the capillary diameter.
- The steady growth stage was the dominant phase for a micrometer scale capillary.
- Gas flow rate mainly affects the gas momentum force and drag force.
- Capillary diameter significantly affects the gas momentum force and surface tension force.

GRAPHICAL ABSTRACT

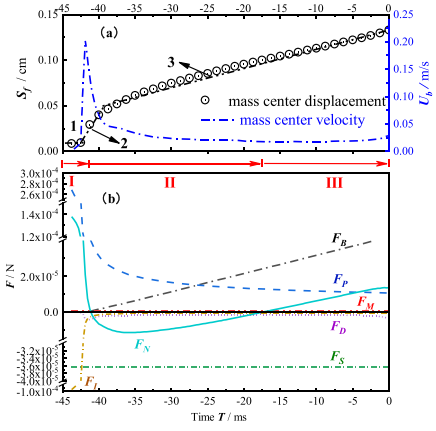

ARTICLE INFO

Keywords:
Bubble formation
Dynamics
micro-capillary
Visual experiment

ABSTRACT

Bubble column offers various advantages compared to other devices in the chemical process industry, which was used as a fine particulate and sulfuric acid mist control device. Bubble formation behaviors, including volume, diameter and velocity, were systematically investigated in the single submerged micro-capillary test bed under constant flow conditions by using the high-speed optical camera in this paper. Besides, force model of the bubble forming process was established based on the experimental results. It was found that the formed bubble turned to be elliptical and bubble shape was independent of the gas flow rate under the conditions of this study. In addition, bubble velocity was found quickly reached the highest level, then decreased, and eventually tended to be stable (0.02–0.1 m/s). By analyzing the bubble forces, it was found that pressure force F_P, surface tension force F_S and buoyancy force F_B played different roles in different bubble formation process. These results can provide detailed parameters for the modeling of bubble formation process under the test conditions.

* Corresponding author.
E-mail address: yunhuang@ipe.ac.cn (Y. Huang).

https://doi.org/10.1016/j.powtec.2023.118258
Received 14 December 2022; Received in revised form 13 January 2023; Accepted 13 January 2023
Available online 16 January 2023

1. Introduction

The bubble formation process is important to many gas-liquid operations that is found in chemical processing, biochemical operations, metallurgy and waste water treatment [1,2]. In most of these applications, bubble formation is accompanied by heat and mass transport processes. Actually, the understanding of bubble behavioral mechanism on transport processes must originate from the research on bubble dynamic behaviors. Basically, the dynamic behaviors of bubbles, especially their formation, interaction and coalescence, depend on capillary diameter, gas flow rate, gas flow pressure, liquid physical properties and so on [3,4]. Up to now, a great number of experimental and simulation studies have been conducted on the behaviors of bubble formation process. For instance, Zhang et al. [5] studied the nonlinear dynamic behaviors of bubbles (formation, interference, collision and coalescence) formed from a submerged orifice with a diameter of 2 mm, and a new comprehensive theoretical model is developed. It was found that the departing period and bubble size were influenced by the wake of previous bubbles. Liu et al. [6] investigated the chaotic bubbling mechanism in a gas-liquid bubble column with a single nozzle with a diameter of 1.2 mm, and the nonlinear bubbling hydrodynamics were studied. It was found that the periodic bubbling gradually developed to random bubbling with increasing gas flow rate. Yang et al. [7] investigated the bubble formation behaviors with a single nozzle with 1.585 mm in diameter, and a model takes into consideration various forces was set up. It was found that the initial bubble size in liquid was determined through the balance of various forces, including buoyancy force, gas momentum force, bubble inertial force, surface tension force, liquid viscous force, and basset force. Kogawa [8] and Saeid [9] observed the bubble formation behaviors in liquid mercury with a micro-capillary with 100–110 μm in diameter. They found that the bubble formation and detachment behaviors on a micro-capillary were quite different from those on a typical millimeter scale capillary. Besides, many studies endeavored to understand the mechanism of the bubble formation process and the influence of processing parameters. Kumar [10] and Lin [11] studied the bubble formation process on a horizontal plate. They found that the contact angle had great influence on the bubble formation process. Davidson [12] showed that the bubble size was approximately proportional to the square root of the orifice diameter. Keitel [13] observed that the bubble size decreased with the addition of small amounts of organic compounds to liquid phase. Most of the above mentioned literatures mainly focused on the bubble dynamic behaviors formed on millimeter scale capillary. However, the bubble formation and detachment behaviors on micrometer scale capillary are quite different from that on millimeter scale [14], such as bubble departure volume, departure time and so on. Few studies had investigated the detailed formation parameters of bubbles formed on micrometer scale capillary. Furthermore, the effect of various forces, involved in bubble formation, on the bubble formation process are not understood.

In this paper, the detailed formation parameters (volume, diameter, velocity, etc) of bubbles formed on a submerged micro-capillary under different flow rates were investigated in the water-air system experimentally. Meanwhile, a force balance model in the bubble formation process was established, and the forces analysis were carried out according to the experimental results. These results can provide necessary information for modeling and simulation of the bubble formation process.

2. Experimental setup

The schematic diagram of bubble formation behaviors on a submerged micro-capillary under constant flow is shown in Fig. 1. The experimental system includes a two-dimensional bubble column, a gas supply system and a real-time photogrammetric measurement system. The bubble column is a transparent polymethyl methacrylate material vessel with a cross-section of 200 × 20 mm and is open to the atmosphere at top. It was filled with de-ionized water to a height of 200 mm unless mentioned otherwise. The depth (20 mm) of the vessel is 1/10 of the width (200 mm) so as to ensure that the bubble pattern has little change along with the depth [15,16]. Besides, the wall effects are negligible since the vessel depth is about 8 times of bubble diameter [17]. A ready-made stainless-steel micro-capillary with precision polishing and clearing (the inset figures in Fig. 1) was fixed at the bottom of the vessel. Four kinds of micro-capillary (Table 1) with different diameters were tested in this experiment. Air was supplied into the micro-capillary by a syringe pump, the line velocity was controlled in a range of 5–50 mm/min. The flow rate was controlled in the range of 0.1–0.2 ml/s, and the actual flow rate Q_G can be calculated experimentally. With the help of a cool lamp (KWS 250 W), a high-speed digital camera (Phantom V311) with a magnification lens (Olympus 5×) was used to record the detailed evolutions of the bubble shape during the bubble formation process, the frame grabbing speed is 3200 frames/s and the resolution is 1280 × 800 pixels. Finally, digital photographs were processed and analyzed by using image processing technology [18].

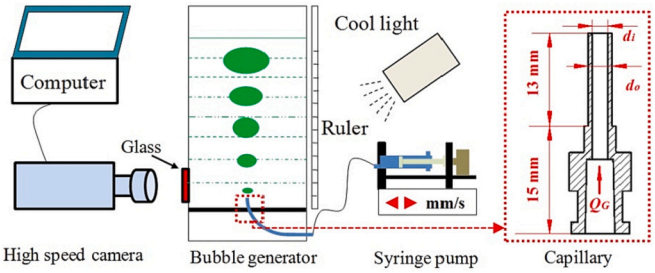

Fig. 1. Schematic diagram of experimental set-up.

3. Force analysis during bubble formation

The bubble formation process is governed by different forces namely buoyancy force F_B, pressure force F_P, gas momentum force F_M, surface tension force F_S, drag force F_D and inertial force F_I [19]. Among all the forces mentioned above, they can be divided into the detaching force and the attaching force according to their effects on the forming bubbles. Among these, the surface tension force, drag force and inertial force serve as an attaching force that hold bubble to the capillary, while the buoyancy force, pressure force and gas momentum force serve as a detaching force that pulls bubble from the capillary. The schematic diagram of the mentioned forces acting on the forming bubble in liquid is shown in Fig. 2 and a brief theoretical description of all these forces is given below.

In the calculation of those forces, the volume of the bubble is a prerequisite. Assume the bubble shape is spherical. Therefore, the buoyancy force F_B acting on the forming bubble of diameter d_b is written as [20]:

$$F_B = \frac{1}{6}\pi(\rho_l - \rho_g)d_b{}^3 g \tag{1}$$

where ρ_l and ρ_g are the densities of liquid and gas respectively, g is the gravitational acceleration constant which is 9.81 m/s^2.

For a bubble completely surrounded by liquid, the net pressure force is zero ($F_P = 0$). However, when the bubble attaches to a surface, the pressure force is unbalanced over the attached area. According to the Young-Laplace equation, the pressure difference between the inside and

Table 1
Parameters for micro-capillary.

	A	B	C	D
Inner diameter d_i mm	0.16	0.33	0.67	1.4
Outer diameter d_o mm	0.31	0.63	1.07	1.8

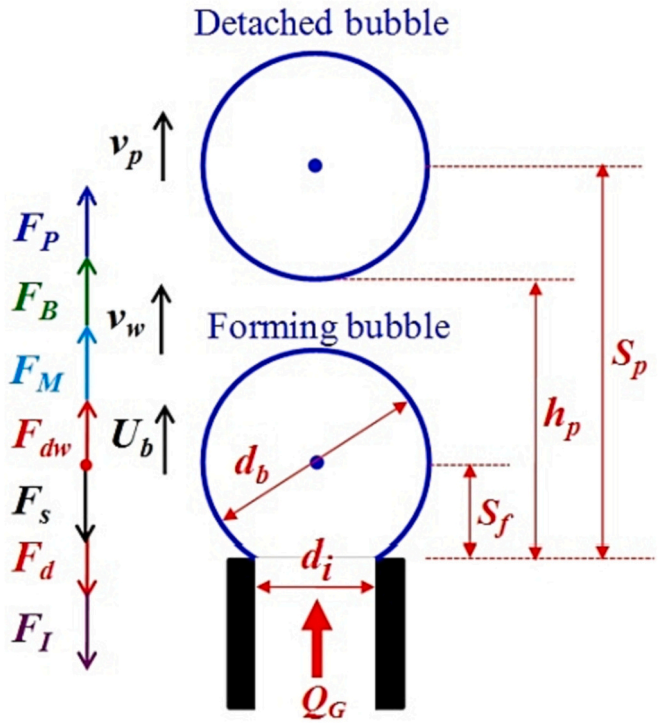

Fig. 2. Schematic diagram of forces acting on the forming bubble.

outside of a bubble is:

$$P_g\text{-}P_l = \frac{4\sigma}{d_b} \tag{2}$$

The pressure force F_P exerted is [21]:

$$F_p = \frac{4\sigma}{d_b}\pi\left(\frac{d_i}{2}\right)^2 \tag{3}$$

where P_l and P_g are the pressures of liquid and bubble gas respectively, σ is the surface tension, d_i is the capillary diameter.

The gas momentum force F_M is due to the flux through the capillary. It can be calculated as [22]:

$$F_M = \rho_g \frac{{Q_G}^2}{(\pi/4){d_i}^2} \tag{4}$$

where Q_G is the constant flow rate. Generally, F_M is small and can be ignored, except at high pressures and at high gas flow rates.

The surface tension force F_S can be written as [9]:

$$F_S = \sigma\pi d_i sin\theta \tag{5}$$

where θ is the supplementary angle of contact angle, and it can be obtained by analyzing the acquired images.

The inertia force F_I is due to the acceleration of bubble and the pertinent liquid, and is expressed as [23]:

$$F_I = Q_G^2\left(\rho_g + \frac{11}{16}\rho_l\right)\frac{{V_b}^{-0.66}}{12\pi\left(\frac{3}{4\pi}\right)^{0.66}} \tag{6}$$

where V_b is the volume of the bubble.

The drag force F_d is due to the move of the bubble with a center velocity U_b can be described as:

$$F_d = \frac{\pi}{4}{d_b}^2 C\frac{\rho_l}{2}{U_b}^2 \tag{7}$$

As the liquid flows by, a shear-lift force is exerted on the bubble due to the velocity difference between two phases, which serves as a drag force. The drag force F_{dw} due to the wake of the previous detached bubble with a impressed velocity ν_w can be described as [24,25]:

$$F_{dw} = \frac{\pi}{4}{d_b}^2 C\frac{\rho_l}{2}{\nu_w}^2 \tag{8}$$

$$\nu_w = \nu_p\left(\frac{S_p - h_p}{h_p - S_f}\right)^{2/3} \tag{9}$$

where ν_p is the velocity of the previous detached bubble, S_p is the distance of the capillary to the previous detached bubble center, h_p is the distance of the capillary to the lower surface, S_f is the distance of the capillary to the forming bubble center.

Combining these two kinds of drag forces to one term, the overall drag force F_D exerted on the forming bubble with can be described as:

$$F_D = F_d + F_{dw} = \frac{\pi}{4}{d_b}^2 C\frac{\rho_l}{2}{U_{eff}}^2 = \frac{\pi}{4}{d_b}^2 C\frac{\rho_l}{2}(U_b - \nu_w)|U_b - \nu_w| \tag{10}$$

where U_{eff} is the relative velocity of the bubble to liquid, C is the drag coefficient of a bubble moving through the liquid phase, the drag coefficient used here is given by:

$$C = \begin{cases} 24/Re_b & 10^{-3} < Re_b < 2, \\ 18.5/{Re_b}^{0.6} & 2 \le Re_b \le 500, \\ 0.44 & 500 < Re_b \le 2\times 10^5. \end{cases} \tag{11}$$

where Re_b is Reynolds number based on bubble diameter, $Re_b = d_b U_{eff}/\gamma_l$ and γ_l is the kinematic viscosity coefficient of the liquid phase. In this paper, the effect of the bubble shape on the drag coefficient was not considered due to the low Reynolds number and small ratio of length to diameter [26], which may lead to a bigger calculation value of bubble drag force than its actual value [27].

Net force F_N acting on the forming bubble is obtained by summing up all the forces from Eqs. (1)–(10) and can be expressed as follows:

$$F_N = F_B + F_M + F_P - F_S - F_I - F_D \tag{12}$$

4. Results and discussion

4.1. Single bubble behavior

In this section, the experiments were conducted at a constant gas flow rate of 1.02 × 10^{-4} cm^3/ms with a micro-capillary diameter of 0.16 mm. The detailed structural parameters of forming bubble versus time are shown in Fig. 3. In this paper, the moment that bubbles detached from the micro-capillary is taken as the origin time ($T = 0$ ms). As

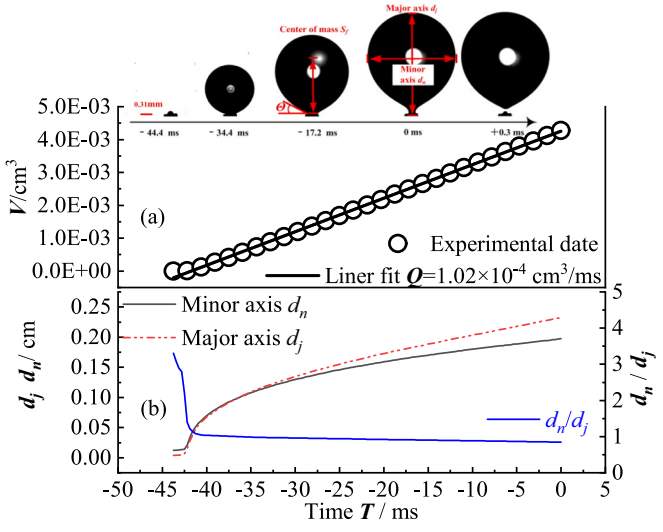

Fig. 3. Structural parameters of forming bubble versus time.

also shown in Fig. 3(a), the bubble volume increases almost linearly with time, which exhibits that the gas flow through micro-capillary is constant. At this gas flow rate, the detached bubble is sufficiently far from the bubble growing at the micro-capillary and the formation of bubble is not influenced by the wake behind the detached bubble, this regime of bubbling is known as the single bubbling regime. As also shown in Fig. 3 (b), the minor and major axis of bubble increase with time and the overall variation trend is the same for both axes. Besides, the growth rate of the major axis is higher than the minor axis. It is also observed that the ratio of the minor axis to the major axis decreases from 3.5 to 0.85, which means that the bubble deforms and turns to be an elliptical shape throughout the bubble formation process.

To better understand the dynamics of bubble formation process, the movement characteristics and forces analysis are conducted in Fig. 4. Fig. 4a shows the evolution of the displacement of bubble mass center. It can be seen that the mass center displacement increases with time and the evolution of the displacement can be divided into three stages. Stage 1 (−45 ~ −42.5 ms): the displacement slowly increases with time. Stage 2 (−42.5 ~ −35 ms): the displacement increases significantly with time. Stage 3 (−35–0 ms): the displacement increases almost linearly with time. The results showed that stage 3 was the dominant phase during the bubble formation process, which was quite different to that performed by Jian [28] with a millimeter diameter capillary. For the millimeter scale diameter capillary, stage 1 was the dominant phase during the bubble formation process. Corresponding to the mass center displacement, the mass center velocity is also present in Fig. 4a. It quickly increases to the highest level, then decreases, and eventually tends to be stable ($U_b \approx 0.025$ m/s). To further understand the change in mass center displacement and velocity during the bubble formation process, the forces acted on bubble are reported in Fig. 4b. It was observed that the forces F_M, F_D, F_S change slightly with time but the forces F_P, F_B, F_I change significantly with time. The net force F_N act on the bubble is also reported in Fig. 4b. Note that the F_N equal to zero at two moments ($T =$ -41 ms and $T = -17.5$ ms) and three regions (labeled I, II, III) can be divided by these two moments. At region I, F_P is obviously larger than F_I, F_S, F_D. Besides, the F_N is greater than zero ($F_N > 0$), which indicates that the bubble moves upwards with increasing velocity. In this region, the F_P tends to pull the bubble from the micro-capillary. The bubble volume increases with time, which gives rise to the rapid decrease of F_P and

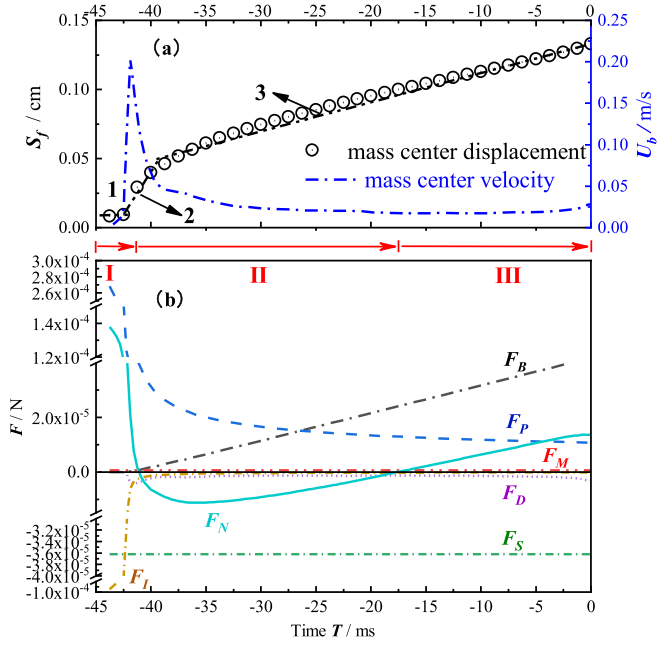

Fig. 4. Movement characteristic (a) and forces analysis (b) of bubble versus time.

gradual increase of F_B. Then the bubble formation process goes into the region II, during which the F_N is less than zero ($F_N < 0$). In this region, the F_S plays a dominating role to hold the bubble to the micro-capillary and dissipate the bubble's kinetic energy. During the final region III, F_N is greater than zero ($F_N > 0$) and F_B is higher than any other forces. The F_B becomes a major force to pull bubbles out of the micro-capillary until the detachment is achieved.

4.2. *Effect of gas flow rate on bubble behavior*

The gas flow rate significantly affects the bubble formation and interaction, leading to various bubbling periods. Therefore, the effects of gas flow rate on bubbling behaviors were investigated with a capillary diameter of 0.16 mm in this part of the paper. At a low gas flow rate, bubbles were formed above the micro-capillary at a regular interval of time (44.4 ms) and this regime of bubbling is known as the single bubbling (Fig. 5a). With an increase in gas flow rate, the bubble formation interval was decreased to 39.4 ms. The shape of the forming bubble above the micro-capillary is affected by the wake behind the leading bubble, especially in the initial stage of bubble formation. There are two bubbles with different volumes coexist in this period and they will not coalesce with each other. This regime is known as the bubbling with pairing (Fig. 5b). With further increase in gas flow rate, the effects of the wake behind the leading big bubble on the forming bubble become so significant that the following small bubble forming at the micro-capillary coalesces with the leading big bubble and forms a bigger one. This regime is known as bubbling with coalescence (Fig. 5c).

Fig. 6a shows the variation of bubble volume at different gas flow rates. The bubble volume almost increases linearly with time and it grows rapidly at a higher gas flow rate before the bubble detaches from the micro-capillary. As mentioned above, when the gas flow rate reaches 1.57×10^{-4} cm^3/ms, the regime of bubbling with coalescence is observed. There are two bubble volumes (A, B) coexist at the same flow rate. Compared with other gas flow rates, the bubble formation period is shorter and the volume of the detached bubble is smaller. Fig. 6b shows the variation of the minor axis at various gas flow rates. The bubble axis increases rapidly at the beginning of bubble formation and maintains a steady growth in the subsequent stages. It is interesting to note that the axis fluctuates slightly with time when the gas flow rate is higher than 1.15×10^{-4} cm^3/ms. This is because the wake behind the detached bubble on the forming bubble becomes so significant in the regime of bubbling with pairing and coalescence (the inset figures in Fig. 6b show the effect of the wake of the detached bubble on the major axis of the forming bubble).

Fig. 7 shows the bubble axis versus bubble volume under various gas flow rates at a given micro-capillary of 0.16 mm, and it can be seen in this figure that the bubble axis increases with bubble volume in a power law. The bubble axis increases rapidly at the beginning of bubble formation and maintains a subsequent steady increase until the bubble detaches from the micro-capillary. It is also observed that the bubble axis is almost the same for a given bubble volume at different gas flow rates in this water-air system. This result indicates that the bubble shape (major and minor axis) is independent of the gas flow rate in the range of gas flow considered in this study.

To better quantify and analyze the effects of gas flow rate on the bubble formation process, the bubble motion parameters are reported in Fig. 8. Fig. 8a shows the variation of bubble mass center displacement S_f under different gas flow rates. It shows that the tendency of S_f changes with increasing gas flow rate. Compared with the process of bubble formation at a low gas flow rate (1.02×10^{-4} cm^3/ms), the S_f increases rapidly with time, and its evolution directly enters the second stage when the gas flow rate is higher than 1.145×10^{-4} cm^3/ms. The measured rise velocity of the forming bubble U_b at different gas flow rates is shown in Fig. 8b. The trend of U_b remains the same over time, rapidly increases to a maximum and then decreases. Besides, a higher gas flow rate leads to a higher U_b at the beginning of the second stage.

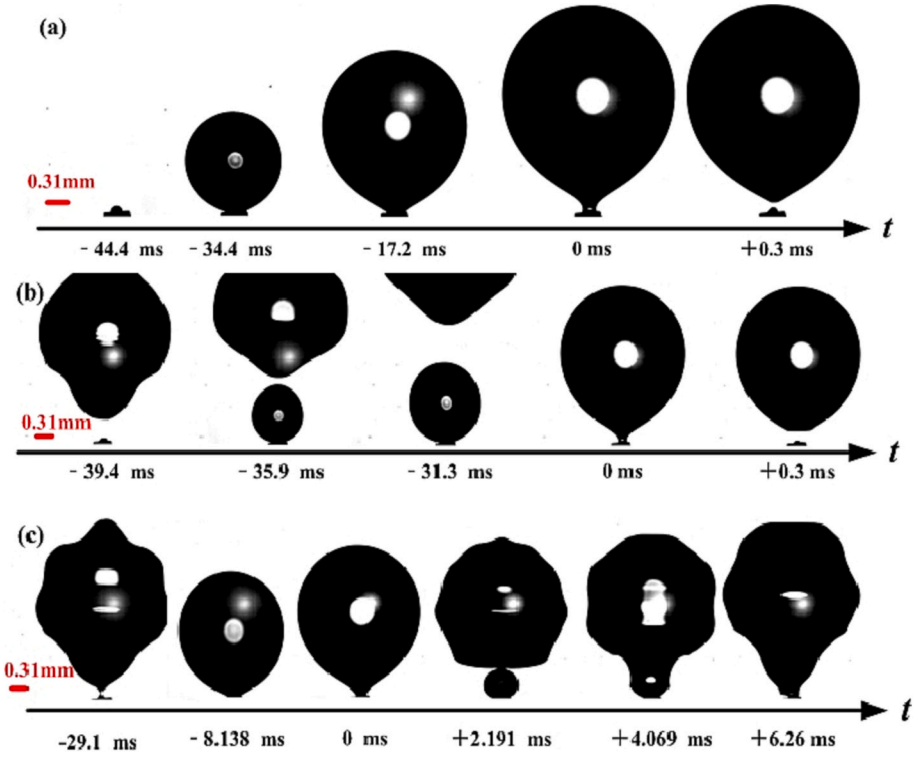

Fig. 5. Regimes of bubble formation: (a) single bubbling (Q = 1.02 × 10^{-4} cm^3/ms) (b) bubbling with pairing (Q = 1.15 × 10^{-4} cm^3/ms) (c) bubbling with coalescence (Q = 1.57 × 10^{-4} cm^3/ms).

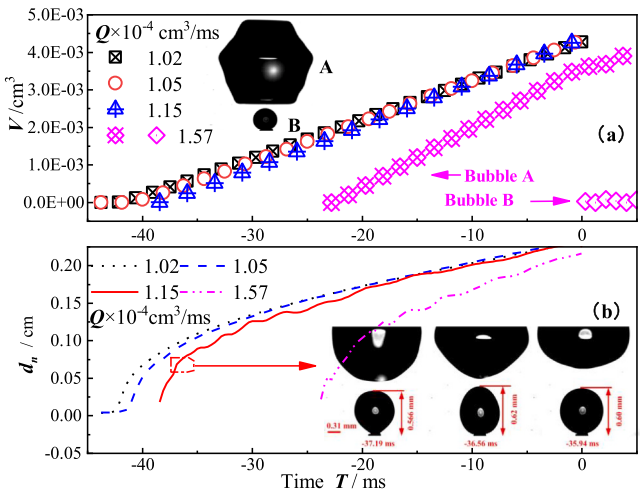

Fig. 6. Structural characteristics of bubble under different gas flow rate.

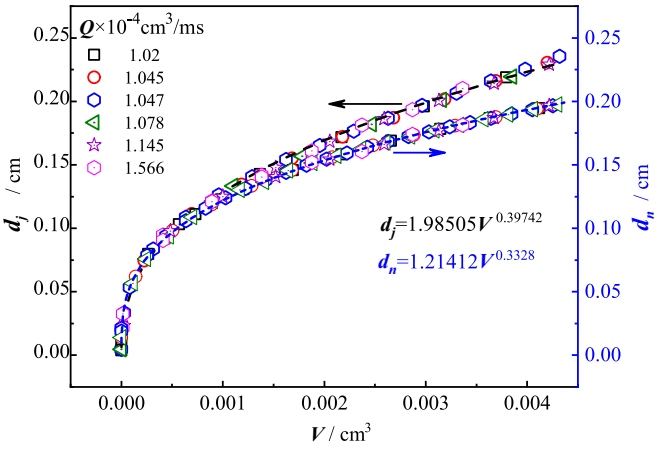

Fig. 7. Variation of bubble axis with bubble volume under different gas flow rates.

When the gas flow rate exceeds 1.15 × 10^{-4} cm^3/ms, the influence of the wake from the previous bubble cannot be neglected. Fig. 8c further shows the variation of the calculated impressed velocity v_w at different gas flow rates. And it reveals that the v_w increases with the increasing gas flow rate. It is also noticeable that the impressed velocity decreases with increasing time. This means that the wake of the previous detached bubble has a significant effect on the beginning stage of bubble formation.

In order to identify and quantify the forces involved in bubble motion under different gas flow rates. It is instructive to first develop a general expression for the total force on a bubble. The variation of forces during the bubble formation process is shown in Fig. 9. It can be seen from these figures, the major differences in forces between these two gas flow rates are F_M and F_D. At larger gas flow rate, the F_M is higher throughout the formation process (Fig. 9a). While the overall drag force F_D is smaller in the first and second regions and bigger in the final region (Fig. 9c). The differences in F_D are mainly caused by the wake of detached bubble. In the first and second regions, the v_w is higher at a larger gas flow rate (as shown in Fig. 8), the relative velocity of bubble to liquid is reduced by the wake of the detached bubble. In the final region, v_w is lower, the effect of detached bubble on the relative velocity of bubble to liquid becomes weak. Fig. 9d shows the net force F_N at two gas flow rates. When the F_N is higher than 0, the bubble was pulled away from the micro-capillary. As shown in this figure, the F_N is higher in lower gas flows at the same bubble volume.

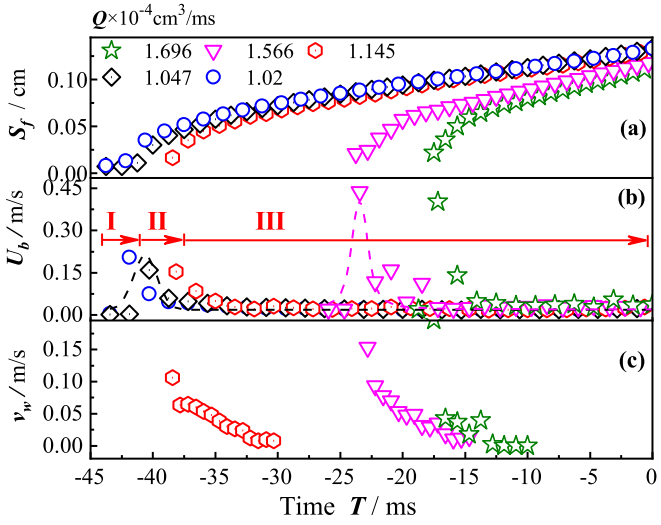

Fig. 8. Displacement (a), velocity (b) and impressed velocity (c) of forming bubble under different gas flow rates.

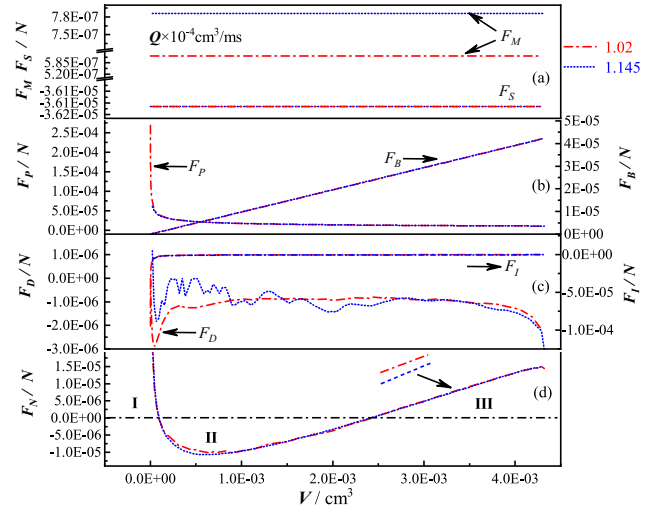

Fig. 9. Forces analysis of bubble under different gas flow rates.

4.3. Effect of micro-capillary diameter on bubble behavior

In this section, the experiments at a gas flow rate of 1.02×10^{-4} cm^3/ms are performed with different capillary diameters. The flow rate was controlled by adjusting syringe pump line velocity and calculated through the experimental data. Under this gas flow rate, the regime of bubbling belongs to the single bubbling process. The variation of minor axis d_n and major axis d_j with bubble volume V under different capillary diameters d_i (0.16, 0.33, 0.67 and 1.4 mm) are shown in Fig. 10a and Fig. 10b, respectively. As shown in Fig. 10a, a power function relation was found between the minor axis and the bubble volume. The minor axis first increases rapidly and then sustains a subsequent steady increase. Besides, it does not vary significantly with the capillary diameters. However, it is also interesting to note that the minor axis increases slightly with the bubble volume at the beginning of the bubble formation process when the capillary diameter is 1.4 mm. This can be attributed to the change of the capillary diameter. These results indicate that the minor axis is restricted by the capillary diameter at the beginning of bubble formation process and the minor axis is independent of the capillary diameter at the end of the bubble formation process. Fig. 10b further shows the major axis versus bubble volume, and it can

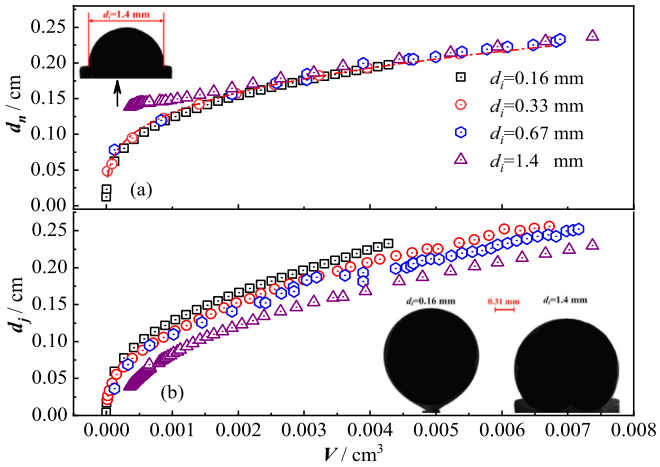

Fig. 10. Variation of bubble axis with bubble volume at different capillary diameters.

be seen that the major axis is smaller with a larger capillary diameter at the same bubble volume (the inset figures in Fig. 10b show the shape of the bubble). The results show that the major axis is sensitive to the changes in capillary diameter, and the bubbles, formed on a larger diameter capillary, have better sphericity. Besides, the volume of the detached bubble increases with the increase of capillary diameter at the same gas flow rate.

Fig. 11 shows bubble mass center and velocity with bubble volume at different capillary diameters. It can be seen that the bubble mass center increases with increasing bubble volume, and the bubble mass center is higher for the capillary with a smaller diameter at the same volume. With regards to the bubble center velocity, it is observed that at the beginning of bubble formation (V<0.002 cm^{-3}), the bubble center velocity quickly reaches a local maximum and then rapidly decreases. Most of the time (V>0.002 cm^{-3}) during the bubble formation process, the bubble rises at a constant velocity. The bubble center velocity is about 0.03 m/s for the capillary with a diameter of 0.67 mm and 0.1 m/s for the capillary with a diameter of 0.33 mm, the center velocity is slightly higher at a smaller diameter capillary. These results indicate the forming bubble center velocity can reach the constant value faster at a bigger diameter capillary, and it can be concluded that the net force of the bubble is higher for the capillary with a bigger diameter.

The bubble forces for capillary with different diameters are given in Fig. 12. As shown in Fig. 12a, the capillary diameter significantly affects the gas momentum force F_M and the surface tension force F_S, and a bigger capillary diameter leads to a higher attaching force that holds the

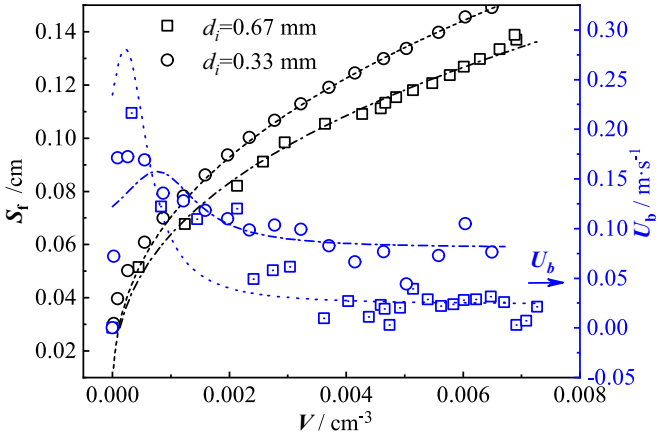

Fig. 11. Variation of bubble mass center and velocity with volume at different capillary diameters.

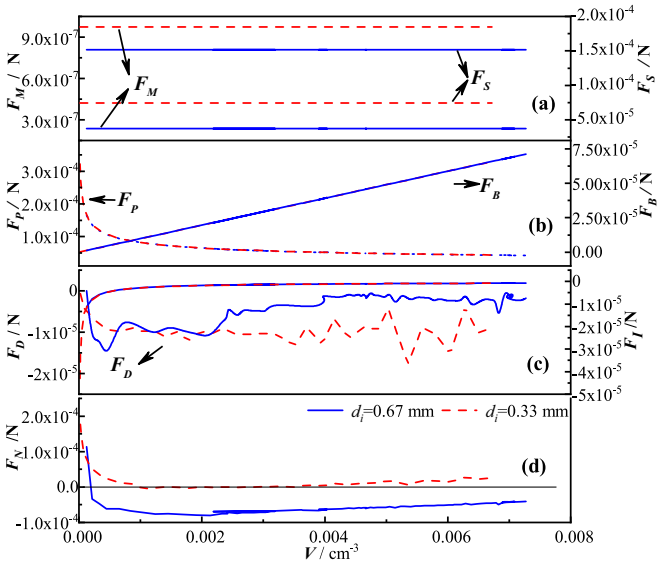

Fig. 12. Bubble forces analysis for capillary with different diameters.

bubble to the larger capillary. Therefore, at the beginning of bubble formation process, a higher pressure force F_P will be applied to balance the attaching force and pull the bubble off the capillary (Fig. 12b). Moreover, it was noted from this figure (Fig. 12d) that the net force F_N trends with bubble volume is the same, and the larger the capillary, the greater the attaching force. When the capillary diameter is 0.33 mm, the bubble volume of $F_N = 0$ is around 0.001 cm^{-3}, which means the bubble center velocity reaches a local maximum at this point. The results are consistent with the drawn conclusions in Fig. 11.

5. Conclusions

The detailed characteristics of bubble formation on a submerged micro-capillary under different flow rate and diameter conditions were investigated in this paper. Besides, the bubble force analysis during the formation process is also conducted based on the experiment data. The following conclusions are obtained:

1) The bubble deforms and turns to be an elliptical form, the growth rate of major axis is higher than minor axis. Besides, the bubble shape is independent of gas flow rate in this water-air system.
2) The velocity of bubble mass center quickly reaches the highest level, then decreases, and eventually tends to be stable ($U_b \approx 0.025$ m/s) in the bubble formation process. Based on the force analysis, Pressure force F_P, surface tension force F_S and buoyancy force F_B are the dominating forces in different formation regions, respectively.
3) The gas flow rate mainly affects the gas momentum force F_M and drag force F_D, leading to various bubble formation stages. The wake of previous detached bubble has a significant effect on the beginning stage of bubble formation.
4) The capillary diameter significantly affects the gas momentum force F_M and the surface tension force F_S, leading to a higher attaching force that holds the bubble to the capillary. Meanwhile, the bubbles, which formed on larger diameter capillary, have better sphericity at same bubble volume.

Credit author statement

Xiang Wang designed the study, analyzed date and wrote the paper. Minhang Song designed the study. Shuiqing Li gave technical support and conceptual advice. Yun Huang supervised the project.

Declaration of Competing Interest

We certify that we have participated sufficiently in the work to take public responsibility for the appropriateness of the calculation method and results. To the best of our knowledge and belief, this manuscript has not been published in whole or in part nor is it being considered for publication elsewhere.

Data availability

Data will be made available on request.

Acknowledgment

This work was supported by the National Natural Science Foundation of China (Grant No. 52006120).

References

[1] R. Lau, R. Mo, S. Wei, Bubble characteristics in shallow bubble column reactors[J], Chem. Eng. Res. Des. 88 (2) (2010) 197–203.
[2] Y. Gao, S. Mitra, et al., Interaction of a spherical particle with a neutrally buoyant immiscible droplet in salt solution[J], Chem. Eng. Sci. 172 (2017) 182–198.
[3] M. Jamialahmadi, M.R. Zehtaban, H. Müller-Steinhagen, et al., Study of bubble formation under constant flow conditions[J], Chem. Eng. Res. Des. 79 (5) (2001) 523–532.
[4] Y. Bo, X. Wu, Y. Zhou, et al., CFD-DPTM-VOF numerical simulation of particle motion and entrainment under the action of single and double bubbles[J], Flow Meas. Instrum. 85 (2022), 102156.
[5] Z. Lei, M. Shoji, Aperiodic bubble formation from a submerged orifice[J], Chem. Eng. Sci. 56 (18) (2001) 5371–5381.
[6] M. Liu, Z. Hu, Studies on the hydrodynamics of chaotic bubbling in a gas–liquid bubble column with a single nozzle[J], Chem. Eng. Technol. 27 (5) (2010) 537–547.
[7] G.Q. Yang, X. Luo, R. Lau, et al., Bubble formation in high-pressure liquid–solid suspensions with plenum pressure fluctuation[J], AICHE J. 46 (11) (2010) 2162–2173.
[8] H. Kogawa, T. Shobu, M. Futakawa, et al., Effect of wettability on bubble formation at gas nozzle under stagnant condition[J], J. Nucl. Mater. 377 (1) (2008) 189–194.
[9] V. Saeid, D. Wen, Bubble formation on a submerged micronozzle[J], J. Colloid Interface Sci. 343 (1) (2010) 291–297.
[10] A. Satyanarayan, R. Kumar, N.R. Kuloor, Studies in bubble formation—I bubble formation under constant flow conditions[J], Chem. Eng. Sci. 24 (4) (1969) 731–747.
[11] J.N. Lin, S.K. Banerji, H. Yasuda, Role of interfacial tension in the formation and the detachment of air bubbles. 1. A single hole on a horizontal plane immersed in water[J], Langmuir 10 (3) (1994).
[12] J.F. Davidson, B.O.G. Schüler, Bubble formation at an orifice in a viscous liquid[J], Chem. Eng. Res. Des. 75 (1) (1997) S105–S115.
[13] G. Keitel, U. Onken, Inhibition of bubble coalescence by solutes in air/water dispersions[J], Chem. Eng. Sci. 37 (11) (1982) 1635–1638.
[14] S.I. Hibino, Bubble formation from an orifice submerged in liquids[J], Chem. Eng. Commun. 22 (1-2) (1983) 63–79.
[15] S. Li, Y. Ding, Y. He, Modelling of the behavior of gas–solid two-phase mixtures flowing through packed beds[J], Chem. Eng. Sci. 61 (6) (2006) 1922–1931.
[16] G.Q. Liu, S.Q. Li, X.L. Zhao, et al., Experimental studies of particle flow dynamics in a two-dimensional spouted bed[J], Chem. Eng. Sci. 63 (4) (2008) 1131–1141.
[17] A.V. Orpe, D.V. Khakhar, Scaling relations for granular flow in quasi-two-dimensional rotating cylinders[J], Phys. Rev. E 64 (3) (2001), 031302.
[18] X. Zhu, J. Xie, Q. Liao, et al., Dynamic bubbling behaviors on a micro-orifice submerged in stagnant liquid[J], Int. J. Heat Mass Transf. 68 (2014) 324–331.
[19] A.A. Kulkarni, J.B. Joshi, Bubble formation and bubble rise velocity in gas− liquid systems: a review[J], Ind. Eng. Chem. Res. 44 (16) (2005) 5873–5931.
[20] A. Bhunia, S.C. Pais, Y. Kamotani, et al., Bubble formation in a co-flow configuration in normal and reduced gravity[J], AICHE J. 44 (7) (1998) 1499–1509.
[21] A.A. Kulkarni, J.B. Joshi, Bubble formation and bubble rise velocity in gas− liquid systems: a review[J], Ind. Eng. Chem. Res. 44 (16) (2005) 5873–5931.
[22] V.K. Badam, V. Buwa, F. Durst, Experimental investigations of regimes of bubble formation on submerged orifices under constant flow condition[J], Can. J. Chem. Eng. 85 (3) (2007) 257–267.
[23] J.F. Davidson, Bubble formation at an orifice in an inviscid liquid[J], Trans. Inst. Chem. Eng. 38 (1960) 335–342.
[24] H. Schlichting, K. Gersten, Boundary-Layer Theory[M], Springer, 2016.
[25] L. Zhang, M. Shoji, Aperiodic bubble formation from a submerged orifice[J], Chem. Eng. Sci. 56 (18) (2001) 5371–5381.

[26] S. Tran, M. Gay, E.E. Michaelides, Drag coefficients of irregularly shaped particles [J], Powder Technol. 139 (1) (2004) 21–32.
[27] M. Rastello, J. Marié, M. Lance, Drag and lift forces on clean spherical and ellipsoidal bubbles in a solid-body rotating flow[J], J. Fluid Mech. 682 (2011) 434–459.
[28] X. Jian, X. Zhu, Q. Liao, et al., Dynamics of bubble formation and detachment from an immersed micro-orifice on a plate[J], Int. J. Heat Mass Transf. 55 (11) (2012) 3205–3213.